

X-RAY EMISSION FROM HESS J1731-347/SNR G353.6-0.7 AND CENTRAL COMPACT SOURCE XMMS J173203-344518

W.W. TIAN^{1,2}, Z. LI³, D.A. LEAHY¹, J. YANG⁴, X.J. YANG⁵, R. YAMAZAKI⁶, D. LU⁴*Draft version January 6, 2010*

ABSTRACT

We present new results of the HESS J1731-347/SNR G353.6-0.7 system from *XMM-Newton* and *Suzaku* X-ray observations, and *Delinha* CO observations. We discover extended hard X-rays coincident with the bright, extended TeV source HESS J1731-347 and the shell of the radio SNR. We find that spatially-resolved X-ray spectra can generally be characterized by an absorbed power-law model, with photon-index of ~ 2 , typical of non-thermal emission. A bright X-ray compact source, XMMS J173203-344518, is also detected near the center of the SNR. We find no evidence of a radio counterpart or an extended X-ray morphology for this source, making it unlikely to be a pulsar wind nebula (PWN). The spectrum of the source can be well fitted by an absorbed blackbody with a temperature of ~ 0.5 keV plus a power-law tail with a photon-index of ~ 5 , reminiscent of the X-ray emission of a magnetar. CO observations toward the inner part of the HESS source reveal a bright cloud component at -20 ± 4 km s⁻¹, which is likely located at the same distance of ~ 3.2 kpc as the SNR. Based on the probable association between the X-ray and γ -ray emissions and likely association between the CO cloud and the SNR, we argue that the extended TeV emission originates from the interaction between the SNR shock and the adjacent CO clouds rather than from a PWN.

Subject headings: (ISM:) supernova remnants-X-rays: observations-radio continuum: galaxy-radio lines-X-rays: individual (HESS J1731-347, SNR G353.6-0.7, XMMS J173203-344518)

1. INTRODUCTION

The concept that astrophysical shock waves are efficient accelerators of cosmic rays have widely been accepted for a long time (Blandford & Eichler 1987; Malkov & Drury 2001). Due to the supernova energetics and rates, it seems reasonable that most of Galactic cosmic rays up to 10^{15} eV originate from supernova remnants (SNRs) shocks accelerating particles (protons and electrons) in the interstellar (ISM) and circumstellar medium (CSM). An efficiency of order 10% of the mechanical energy in the shocks must go into accelerating protons and nuclei to explain the observed intensity of cosmic rays. However, the relative efficiency of acceleration of protons vs. electrons as well as the maximum energies obtained are not well understood, but are all fundamental to the study of cosmic rays and their effects on the ISM.

Recently X-ray and γ -ray observations to SNRs, e.g. SN1006, RX J1713.7-3946 and Vela Junior (RX J0852.0-4622 etc) have revealed that SNR shocks are able to accelerate particles to TeV energies (Enomoto et al. 2002; Aharonian et al. 2006). The high energy particles responsible for emitting TeV photons can be either hadrons or leptons, which are produced in astrophysical accelerators as in SNRs. Two primary TeV photon emission processes are the decay of neutral pions produced by interac-

tions of hadronic particles (mostly protons) with ambient matter and the inverse-Compton scattering of electrons on ambient photons (mostly the micro-wave background radiation in the typical ISM). The particles, which undergo such energy losses, do not escape the acceleration and emission sites due to the presence of magnetic fields. However, the TeV photons escape directly, allowing us to explore the sites of these processes.

The High Energy Stereoscopic System (HESS), with its excellent sensitivity and spatial resolution in the standard of γ -ray astronomy, greatly stimulates studies of very high energy astrophysics in recent years. A multi-wavelength approach has proven to be robust in shedding light on the nature of TeV sources. Among well-identified radio/X-ray counterparts of about 30 Galactic TeV sources⁷, young shell-type SNRs and pulsar wind nebulae are thought to be two major γ -ray generators (Bamba et al. 2003; Katagiri et al. 2005; Aharonian et al. 2006; Uchiyama et al. 2007; Chang et al. 2008; Camilo et al. 2009). Other candidates have also been proposed as counterparts of some unidentified TeV sources, e.g., old SNRs (Yamazaki et al. 2006; Fang & Zhang 2008), hypernova and γ -ray burst remnants (Ioka & Meszaros 2009), giant molecular clouds (Butt et al. 2008; Bamba et al. 2009), and young stellar clusters (Aharonian et al. 2007). Recently, the extended TeV source HESS J1731-347 is found to almost entirely overlap an old radio/X-ray SNR candidate G353.6-0.7 (Aharonian et al. 2008; Tian et al. 2008, hereafter T08). The association between HESS J1731-347 and G353.6-0.7, as suggested by T08, makes this system a favorable laboratory for studying the generation of γ -rays

¹ Department of Physics & Astronomy, University of Calgary, Calgary, Alberta T2N 1N4, Canada, wtian@ucalgary.ca

² National Astronomical Observatories, CAS, Beijing 100012, China; tww@bao.ac.cn

³ Harvard-Smithsonian Center for Astrophysics, 60 Garden Street, Cambridge, MA 02138, zyli@head.cfa.harvard.edu

⁴ Purple Mountain Observatory, CAS, Nanjing 210008, China

⁵ Department of Physics, University of XiangTan, China

⁶ Department of Physical Science, Hiroshima University, Higashi-Hiroshima 739-8526, Japan

⁷ <http://tevcat.uchicago.edu/>, <http://www.mppmu.mpg.de/~rwagner/sources>

in evolved SNRs. T08 considered the case of hadronic particle acceleration in an SNR shock encountering a dense molecular cloud, based on the theoretical model (Yamazaki et al. 2006), but conclusion remained to be drawn due to limitation of the data explored in their paper, i.e., low counting statistics of the *ROSAT* observation and the lack of high-resolution ^{12}CO maps. In this paper, we report new results obtained from *XMM-Newton* and *Suzaku* X-ray observations and CO spectral-line data from Delinha 13.7 m radio telescope, and examine the theoretical model.

2. X-RAY AND RADIO OBSERVATIONS

2.1. XMM-Newton and Suzaku Data

HESS J1731-347 was observed by *XMM-Newton* on March 21, 2007 (ObsID 0405680201; PI: G. Puehlhofer), with a 25 ksec exposure. We reduced the data obtained from the European Photon Imaging Camera (EPIC), using the *XMM-Newton* Science Analysis System (SAS), version 8.0. We selected EPIC-MOS and EPIC-pn events with patterns 0-12 and 0-4, respectively. An examination of the light curve indicated that the observation was contaminated by background flares. Cleaning of the high particle background results in effective exposure of 15.9, 11.8 and 6.2 ks for the MOS1, MOS2 and pn detectors, respectively. Moreover, the observation was also contaminated by straylight⁸, presumably from a bright source, 1RXS J173157.7-335007 (Voges et al. 1999), located at $\sim 50'$ off axis to the north and outside the field of view (FoV). Consequently, a substantial portion of the upper (northern) FoV of the MOS1 and pn detectors was contaminated (contamination in the MOS2 FoV is apparently minimal) and thus masked out from subsequent analysis. We produced counts and exposure maps for the three detectors, in the 0.8-1.5, 1.5-2.2 and 2.2-7 keV bands. The low energy cutoff is justified by the relatively high foreground absorption near the Galactic plane. We then merged the counts and exposure maps, accounting for the difference in the effective area among the three detectors. We also produced corresponding background maps, using the Filter Wheel Closed data that characterizes the quiescent particle background.

HESS J1731-347 was observed by *Suzaku* on Feb. 23, 2007 (ObsID 401099010; PI: G. Puehlhofer), with both X-ray Imaging Spectrometers (XIS) (Koyama et al. 2007) and Hard X-ray Detector (Takahashi et al. 2007). The net exposure time is about 33 ks. In this work, we focus on the XIS Front-Illuminated (FI) CCDs that have very high efficiency and low background especially around 5 keV. Since the XIS2 became inoperable since November 2002, only data from XIS0 is used here. We used cleaned version 2.0 data (reduction by HEADAS software version 6.5). The *Suzaku* FoV is 18×18 arcmin², centered at a bright compact source [$17^{\text{h}}32^{\text{m}}10^{\text{s}}$, $-34^{\circ}46'$]. The *Suzaku* spectra were extracted from a circular-source region with off-source annulus background region in the same observation so that possible contamination by SNR emission is reduced to the minimum. In order to increase the statistics, the spectra from XIS0 and XIS3 were jointly fitted for subsequent analysis.

2.2. CO Data

We observe the G353.6-0.7/HESS J1731-347 system by employing the 13.7 meter Delinha millimeter telescope at the Purple Mountain Observatory in March 2008. The telescope has an angular resolution of $55''$ at the observing frequencies. Simultaneously the three J=1-0 CO isotopic lines (i.e., ^{12}CO , ^{13}CO , and ^{18}CO) were observed by using a cryogenic superconducting SIS receiver and a multi-line backend spectroscopic system (Zou et al. 2004), but only the ^{12}CO was bright enough for significant detection. The system provides a velocity coverage from $V_{\text{LSR}} = -150$ to 60 km s^{-1} and velocity resolution of 0.37 km^{-1} in ^{12}CO . Three target spots (see Fig.1b), each with a size of $5' \times 5'$, were selected over the G353.6-0.7 area, which includes the center position at the TeV γ -ray peak (S1:[RA=17:32:00, Dec=-34:42:00]), and the *ROSAT* X-ray peak sites (S2: [173220, -345400], S3:[173250, -344600]), respectively. These regions were mapped with a grid size of $1' \times 1'$. Each point was integrated up to 6 minutes, resulting an average rms noise level in the spectra to be 0.2-0.3 K. Spectral line data were processed by the CLASS package of GILDAS software developed by IRAM.

3. RESULTS

3.1. X-ray emission

3.1.1. X-ray morphology

Fig. 1 shows the overall X-ray morphology revealed by *XMM-Newton*, along with the radio continuum emission of G353.6-0.7 (Fig. 1a) and the γ -ray emission of HESS J1731-347 (Fig. 1b). The radio SNR has a shell-like morphology and an extent of $\sim 30'$ in diameter, largely overlapping the extended HESS source. On the eastern half of the SNR, X-ray emission coincident with the radio emission was detected in an early *ROSAT* observation (T08). This is confirmed by the present *XMM-Newton* observation, although the lower (southern) part of the radio shell falls outside the *XMM-Newton* FoV. It is also evident that X-ray emission is present along the western half of the radio shell, which was not detected in the *ROSAT* observation albeit its larger FoV. This can be understood, as the emission is detected only in the 2.2-7 keV band that is almost entirely beyond the *ROSAT* energy coverage.

A number of X-ray substructures are revealed under the moderate spatial resolution of *XMM-Newton*. In particular, a prominent filament is present within the shell, passing through the brightest (inner) part of the HESS source (Fig. 1b) and partially coincident with radio continuum emission (Fig. 1a). With comparable widths of $\sim 2'$, the filament and the eastern X-ray shell together define a ring-like feature (enclosed by the two dotted circles in Fig. 1a; hereafter referred to as the ring), along which there are several bright knots (highlighted by the small ellipses in Fig. 1a). Several plumes are present northwest of the ring, where the radio shell apparently breaks. From their projected positions, it is not clear whether the plumes are the natural extent of the shell or the filament. Furthermore, there is a bright compact source centering at (R.A., Dec.) = ($17^{\text{h}}32^{\text{m}}03^{\text{s}}$, $-34^{\circ}45'18''$), showing no counterpart on the radio image. This source is named XMMS J173203-344518 hereafter.

The ring is not necessarily a coherent feature. Nev-

⁸ http://xmm.esac.esa.int/external/xmm_user_support/documentation/uhb/node23.html

ertheless, subsequent analysis is focused on the X-ray emission along the ring, as it occupies the central portion of the *XMM-Newton* FoV that is not subject to the straylight contamination. Fig. 2 shows the azimuthal distribution of the X-ray emission along the ring. Individual peaks, e.g., at position angles of $\sim 120^\circ$, 190° and 230° , arise from the bright knots (hereafter referred to as K1, K2 and K3). The ring appears harder on its western half (i.e., the filament, in angular range of 0° - 180°) than on its eastern half (i.e., the shell).

3.1.2. X-ray spectra

We will focus on the *XMM-Newton* data because Suzaku XIS has a smaller FoV and a lower spatial resolution (~ 1.8 arcmin) than that of the *XMM-Newton*. We extract spectra, based on the MOS1, MOS2 and pn data, from various regions along the ring, including the three knots, the eastern half of the ring (K2 and K3 excluded), and the western half of the ring (i.e., the filament, K1 excluded). As the SNR fills almost the entire FoV, an ideal selection of local background is not possible. We choose to adopt a background spectrum from a 2/5-radius concentric circle within the ring, where the intensity appears to be among the lowest values across the FoV. Given the high intensities along the ring, our background adoption is not expected to introduce significant bias to the spectral fit. An absorbed power-law model is found to be an acceptable characterization for almost all the spectra, resulting in absorption column densities of $\sim 10^{22}$ cm $^{-2}$ and photon-index of ~ 2 , typical of non-thermal emission. The only exception is the spectrum of the eastern ring (i.e., the shell), for which the power-law model, with a steeper photon-index of ~ 2.7 , is not satisfactory fit. Fitting the ER spectra with a thermal or thermal+PL model does not lead to a better fit, hence we present the PL model fit for consistency with other spectra. The MOS2 spectrum of the plumes northwest to the ring (Fig. 1a; the MOS1 and pn data at this region are contaminated by straylight) can also be fitted by a power-law with the index of about 2.2, but subject to large uncertainty due to the limited counts. The fit results are summarized in Table 1. Selected spectra and the best-fit models are shown in Fig. 3. All the spectra are binned to achieve a signal-to-noise ratio greater than 4 (and a minimum of 30 counts per bin), ranging from about 50 to 350 bins.

We also extract spectra for XMMS J173203-344518 from both the *XMM-Newton* and *Suzaku* XIS data. The simple pure absorbed power-law model gives a steep photon index, i.e. ~ 5.1 for the *XMM-Newton* spectra and ~ 4.7 for the *Suzaku* spectra. However, the compact source spectra from both the *XMM-Newton* and *Suzaku* are better fitted by a combined model (i.e., blackbody plus power-law or two blackbodies). When the *XMM-Newton* and *Suzaku* data were fitted independently, the temperatures were found to be consistent with being equal (~ 0.5 keV). To better constrain spectral parameters we jointly fit the *XMM-Newton* and *Suzaku* spectra. For this joint-fit the column density and temperature were set equal for the *XMM-Newton* and *Suzaku* spectra (the power-law photon-index is tied for both spectra also); all other parameters were independent. Both the blackbody plus power-law fit ($\chi^2/\text{d.o.f.}=252/260$) and

the two blackbodies fit ($\chi^2/\text{d.o.f.}=249/260$) are good fits. We show the spectra and the blackbody plus power-law best-fit model in the bottom panels of Fig. 3. The fit parameters are given in Table 2. The compact source shows intrinsic flux in the *Suzaku* observation a little higher than in the *XMM-Newton* observation. We discuss the nature of this source in § 4.

3.2. CO spectra

The three CO spectra (S1: J173200-344200; S2: J173220-345400; S3: J173250-344600) all show several bright cloud components (Fig. 4). Given a near kinematic distance of ~ 3.2 kpc for G353.6-0.7, as inferred from the highest HI absorption feature at a velocity of $\sim -20 \pm 4$ km s $^{-1}$ (T08), these CO spectra reveal increasing H $_2$ column density (~ 2 , 3 and 6×10^{21} cm $^{-2}$ for S2, S3 and S1, respectively; see discussion section) towards the Galactic plane. A bright cloud component at -20 ± 4 km s $^{-1}$ appears in the direction of S1 (i.e. near the intensity peak of the HESS source). This cloud is likely in front of the SNR and extends to the nearby bright HII region G353.42-0.37 to produces the deep HI absorption feature at -20 ± 4 km s $^{-1}$ seen in the HI absorption spectrum from G353.42-0.37. Therefore it is plausible that the extended CO cloud is associated with the remnant and locates at same distance of ~ 3.2 kpc as the HII region.

4. DISCUSSION AND CONCLUSION

4.1. Nature of XMMS J173203-344518

A number of Galactic TeV objects are suggested to be PWNe (Kargaltsev & Pavlov 2008; Gaensler & Slane 2006). In view of the proximity between XMMS J173203-344518 and the projected centers of HESS J1731-347 and SNR G353.6-0.7, it is worth considering a PWN origin for the γ -ray emission. In § 3 we described that the spectra of XMMS J173203-344518 can be approximated by a power-law model with a photon index of 4 - 5, which is much steeper than the typical values of PWNe ~ 1.5 - 2.1 (Li et al. 2008). Neither is this index reminiscent of background active galactic nuclei or Galactic X-ray binaries, whose spectra, when fitted with a power-law model, show typical photon-index of ~ 1.5 - 2. In addition, XMMS J173203-344518 has no radio counterpart and no extended morphology. The above facts strongly argue against a possible PWN origin for the HESS source.

The source's spectra show a harder X-ray tail in the *Suzaku* observation than in the *XMM-Newton* observation (Fig. 3), so the source is a little brighter in the *Suzaku* image than in the *XMM-Newton*. We have excluded the possible contamination by the SNR emission, so the flux variability seems be real (the *Suzaku* observation is 26 days later than the *XMM-Newton*'s). This X-ray variability is possibly consistent with that of a cataclysmic variable (CV) (Pretorius & Knigge 2007). We have examined the intra-observation (tens of ks in duration) light curves of the source but found no evidence for a flux variation, although we note that CVs do show X-ray variability on longer timescales. XMMS J173203-344518 does not appear in the CVs catalog⁹.

On the other hand, it is not implausible that XMMS J173203-344518 is the central compact object (CCO)

⁹ 2006 version: <http://heasarc.nasa.gov/W3Browse/all/cvcat.html>

associated with SNR G353.6-0.7. Typically found in young SNRs, CCOs are characterized by blackbody-like soft X-ray emission with temperatures of 0.2-0.5 keV (Pavlov et al. 2004). It is suggested that CCOs are neutron stars born in supernova explosions with properties different from those of classical rotation-powered pulsars (Gotthelf et al. 2005; Li 2007). XMMS J173203-344518 shows a blackbody temperature (~ 0.5 keV) higher than most CCOs. We think that it is possibly a magnetar (i.e. AXPs and SGRs), because magnetars have soft spectra, a typical blackbody temperature of ~ 0.5 keV and a typical luminosity of 10^{34-36} erg s $^{-1}$ (Mereghetti 2008), also see a magnetar Catalogue¹⁰. Given a distance of ~ 3.2 kpc, if XMMS J173203-344518 is associated with the SNR, it will have a 1-10 keV luminosity of $\sim 10^{34}$ erg s $^{-1}$. This perhaps means it is like AXPs more than SGRs, because SGRs usually have luminosities higher than AXPs, and this source so far shows no repeated soft γ -ray emission. We examine the *XMM-Newton* and Suzuka light curves of XMMS J173203-344518 and find no evidence for pulsations at frequencies between 0.05-1 Hz, a range typical of magnetars. Although magnetars often show a hard X-ray (tens of keV) tail that can be fitted by a shallow power law model, no counterpart of XMMS J173203-344518 is found in the INTEGRAL/ISGRI map (in the energy range of 20-40 keV) and INTEGRAL/JEMX map (3-15 keV). In addition, we notice that there is a little higher column density in the direction of XMMS J173203-344518 than from other regions of SNR G353.6-0.7 (see Table 1). This may be caused by a local dense cloud. Future X-ray observations are needed to test the magnetar scenario for XMMS J173203-344518.

4.2. X-ray and γ -ray emission mechanism

Based on a statistics of 5 young SNRs, the typical photon index of $\sim 2.1 - 3.7$ for non-thermal SNRs has been suggested (Bamba et al. 2005). It is interesting that the hard X-ray emission of the ring in the HESS J1731-347/SNR G353.6-0.7 has similar photon index of ~ 2.2 . But the SNR is old due to its extended (~ 30 arcmin in diameter) and faint radio emission (T08) so it should have a different high-energy mechanism. Old SNRs have quite different characteristics for the expected broad-band energy spectrum of accelerated electrons and protons than young SNRs (Yamazaki et al. 2006). As an SNR ages, the acceleration time increases, allowing higher maximum energy of accelerated particles. However the losses also increase with time. The net result is that the electron spectrum is loss-limited when the SNR is older than $\sim 10^3$ yr, but the proton spectrum only becomes loss-limited when the SNR is older than $\sim 10^5$ yr. Therefore, in an old SNR, the γ - and X-ray emissions are expected to be dominated respectively by decay of neutral pions and by synchrotron radiation of secondary electrons from charged pion decay, respectively. These pions all result from collisions of primary protons and the ISM. One diagnostic is the ratio of TeV to X-ray synchrotron fluxes. If the protons are accelerated at the shock running into a GMC, for example, the ratio should then be $\lesssim 10$, consistent with the value obtained for HESS J1834-087 (Tian et al. 2007). In contrast, if the cloud is only

illuminated by the particles, the predicted ratio should then be greater than 100, due to the lack of magnetic field enhancement which would occur in the shock case (hence greatly enhancing the X-ray synchrotron emission).

Based on the best-fit models (Table 1), the 2-10 keV unabsorbed flux from the ring (including the three knots) is found to be $\approx 6.9 \times 10^{-12}$ ergs cm $^{-2}$ s $^{-1}$. The γ -ray flux is $F_{\gamma(1-10\text{TeV})} \approx 1.7 \times 10^{-11}$ ergs cm $^{-2}$ s $^{-1}$ in the 1-10 TeV band, so the ratio $R = F_{\gamma}/F_X$ is ~ 2.5 . A slightly lower value of R is expected if the X-ray emission from the heavily absorbed western-shell is also considered.

For an old SNR ($\sim 10^4$ yrs for SNR G353.6-0.7), a theoretical model shows that the flux in the 1-10 TeV band is a few times higher than that in 2-10 keV band if the TeV emission is from pion-decays, the X-rays are from synchrotron emissions of secondary electron (in the case of a shocked GMC). Synchrotron emissions from secondary electrons are about 3 orders of magnitude higher than that from primary electrons. Thermal X-ray emission is not considered in this model. However, there is little thermal emission originating from an old SNR.

The new Fermi large Area Telescope survey released a strong γ -ray source table in the range of 100 MeV - 100 GeV (Abdo et al. 2009). There is no strong GeV source within HESS J1731-347. For a case that TeV γ -ray and X-ray emissions originate from a shocked GMC, the GeV emission flux is about 2 orders of magnitude lower than that the TeV flux (Fig. 5 of Yamazaki et al.) which is much low comparing with other cases (Figs. 2-6 of Yamazaki et al.), consistent with the explanation above.

New CO observations support such an SNR scenario: an extended CO cloud at ~ 20 km s $^{-1}$ is associated with the SNR. From the spectrum of S1, we estimate an approximate H $_2$ column density of $\sim 4 \times 10^{21}$ cm $^{-2}$ within the cloud, taking X factor of $\sim 2.5 \times 10^{20}$ cm $^{-2}$ K $^{-1}$ km $^{-1}$ s (Solomon & Barrett 1991). Assuming the molecular cloud completely covers the SNR (at least over the extended HESS source region), then it has a mass of $M_{H_2} = N_{H_2} \Omega d^2 (2m_H/M_{\odot}) \approx 5 \times 10^4 M_{\odot}$. This is a GMC. S1 is located at the peak area of TeV source, and has a higher local H $_2$ column density than S2 and S3. This is consistent with the model of a shocked GMC. The evidence of increasing column density from lower-latitude region to higher-latitude region of the SNR revealed by the CO spectra give a plausible reason on the X-rays distribution. The ROSAT X-ray image of SNR G353.6-0.7 in the soft band (0.1-2.4 keV) appears only within the lower-latitude half of the radio remnant where the N_H is less than 10^{22} cm $^{-2}$ (e.g. S3 and S2) because absorption blocks soft X-rays but not hard X-rays from the upper half where the N_H is larger than 10^{22} cm $^{-2}$. From the viewing-angle of observers, this gives a physical image that the GMC covers the SNR, so the TeV emissions cover the X-ray and radio emission regions. The coincidence of the X-ray morphology with both the radio and TeV γ -ray morphologies suggests that they are physically associated.

WWT and DL acknowledge support from the Natural Sciences and Engineering Research Council of Canada. We thank Drs. A. Bamba, C. Heinke and S. Zhang for their help on analyzing Suzaku and INTEGRAL data. RY was supported in part by a Grant-in-aid from the

¹⁰ <http://www.physics.mcgill.ca/pulsar/magnetar/main.html>

Ministry of Education, Culture, Sports, Science, and Technology of Japan (No. 21740184). Upon the submission of our manuscript, we became aware of the recent

work by Acero et al. (2009) on the HESS J1731-347/SNR G353.6-0.7 system with independent approaches.

REFERENCES

- Abdo, A.A., Ackermann, M., Ajello, M. et al. 2009, *ApJS*, 183, 46
 Acero, F., Philhofer, G., Klochkov, D. et al. 2009, *Proc. 31st Int. Cosmic Ray Conf.*, in press, arXiv:0907.0642
 Aharonian, F., Akhperjanian, A.G. et al. 2006, *ApJ*, 636, 777
 Aharonian, F., Akhperjanian, A.G., Bazer-Bachi, A.R. et al. 2007, *A&A*, 467, 1075
 Aharonian, F., Akhperjanian, A.G., Barres de Almeida, U. et al. 2008, *A&A*, 477, 353
 Bamba, A., Yamazaki, R., Kohri, K. et al. 2009, *ApJ*, 691, 1854
 Bamba, A., Yamazaki, R., Yoshida, T. et al. 2005, *ApJ*, 621, 793
 Bamba, A., Yamazaki, R., Ueno, M., Koyama, K. 2003, *ApJ*, 589, 827
 Blandford, R., Eichler, D. 1987, *Phys. Rep.*, 154, 1
 Butt, Y.M., Schneider, N., Dame, T.M., Brunt, C. 2008, *MNRAS*, 385, 1764
 Camilo, F., Ransom, S.M., Gaensler, B.M., Lorimer, D.R., 2009, *ApJ*, 700, 34
 Chang, C., Konopelko, A., Cui, W. 2008, *ApJ*, 682, 1177
 Enomoto, R., Tanimori, T., Naito, T. 2002, *Nature*, 416, 823
 Fang, J., Zhang, L. 2008, *MNRAS*, 384, 1119
 Gaensler, B.M., Slane, P.O. 2006, *Ann.Rev.Astr.Ap.*, 44,17
 Gotthelf, E.V., Halpern, J.P., Seward, F.D. 2005, *ApJ*, 627, 390
 Ioka, K., Meszaros, P. 2009, accepted by *ApJ*, see arXiv0901.0744
 Katagiri, H., Enomoto, R., Ksenofontov, L.T. et al. 2005, *ApJ*, 619, 163
 Kargaltsev, O., Pavlov, G.G. 2008, *AIPC*, 983, 171
 Koyama, K., Tsunemi, H., Dotani, T. et al. 2007, *PASJ*, 59, 23
 Li, X.D. 2007, *ApJ*, 666, L81
 Li, X.Y., Lu, F.J., Li, Z. 2008, *ApJ*, 682, 1166
 Malkov, E., Drury, L.O'C. 2001, *Rep. Prog. Phys.*, 64, 429
 Mereghetti, S. 2008, *A&ARv*, 15, 225
 Pretorius, M.L., Knigge, C. 2007, *A&A*, 2007, 461, 1103
 Pavlov, G. G., Sanwal, D., Teter, M.A. 2004, *IAUS*, 218, 239
 Solomon, P.M., Barrett, J.W. 1991, *IAUS*, 146, 235
 Takahashi, T., Abe, K., Endo, M. et al. 2007, *PASJ*, 59, 35
 Tian, W.W., Leahy, D.A., Haverkorn M., Jiang, B. 2008, *ApJ*, 679, L85
 Tian, W.W., Li, Z., Leahy, D.A., Wang, Q.D. 2007, *ApJ*, 657, L25
 Uchiyama, Y., Aharonian, F.A., Takahashi, T. et al. 2007, *Nature*, 449, 576
 Voges, W., Aschenbach, B., Boller, Th. et al. 1999, *A&A*, 349, 389
 Yamazaki, R., Kohri, K., Bamba, A. et al. 2006, *MNRAS*, 371, 1975
 Zuo, Y.X., Yang, J., Shi, S.C. et al. 2004, *ChJAA*, 4, 390

TABLE 1
SPECTRAL FIT RESULTS FROM *XMM-Newton* IMAGE

Parameter	K1	K2	K3	ER	WR
$\chi^2/d.o.f.$	29/22	147/109	79/77	88/54	155/165
N_H (10^{22} cm $^{-2}$)	$1.44^{+0.55}_{-0.26}$	$1.21^{+0.15}_{-0.12}$	$0.86^{+0.11}_{-0.11}$	$1.08^{+0.19}_{-0.17}$	$1.85^{+0.20}_{-0.16}$
Photon index	$1.98^{+0.44}_{-0.22}$	$2.15^{+0.14}_{-0.13}$	$2.25^{+0.15}_{-0.15}$	$2.72^{+0.29}_{-0.26}$	$2.39^{+0.16}_{-0.13}$
Norm (PL; 10^{-4})	$1.1^{+0.9}_{-0.3}$	$5.3^{+1.1}_{-0.8}$	$4.3^{+0.9}_{-0.7}$	12^{+5}_{-3}	25^{+6}_{-4}
Flux $_{2-10\text{keV}}$ (10^{-13} ergs s $^{-1}$ cm $^{-2}$)	2.8	11.0	7.8	11.5	36.3

NOTE. — Regions of spectral interest: K1, K2 and K3 -three bright knots; ER - the eastern half of the ring excluding K2 and K3; WR - the western half of the ring excluding K1; See details in text. Quoted uncertainties are at 90% confidence level. An absorbed power-law model is used to fit all spectra.

TABLE 2
SPECTRAL FIT RESULTS FROM THE X-RAY COMPACT SOURCE

Parameter	BB ^a	PL ^a	BB+PL ^a	BB+BB ^a	BB+PL ^b	BB+BB ^b
$\chi^2/d.o.f.$	120/78	118/78	76/78	82/78	252/260	249/260
N_H (10^{22} cm $^{-2}$)	1.36 ± 0.06	3.20 ± 9.09	2.56 ± 0.24	1.53 ± 0.08	$2.80^{+0.26}_{-0.26}$	$1.96^{+0.27}_{-0.22}$
Photon index ...		4.69 ± 0.08	4.40 ± 0.32		$4.84^{+0.48}_{-0.38}$	
Norm (PL; 10^{-2})		5.27 ± 0.56	1.91 ± 0.91		$^c 2.41^{+1.41}_{-0.93} / ^d 2.38^{+1.50}_{-0.96}$	
Temp ₁ (keV)	0.52 ± 0.01		0.48 ± 0.03	0.47 ± 0.02	$0.50^{+0.02}_{-0.02}$	$0.31^{+0.07}_{-0.05}$
Norm ₁ (BB)	9.51 ± 0.87		9.21 ± 3.35	14.92 ± 2.51	$^c 6.0^{+2.0}_{-1.6} / ^d 9.1^{+2.9}_{-2.3}$	$^c 73.9^{+171}_{-46.2} / ^d 71.5^{+165}_{-43.5}$
Temp ₂ (keV)				2.37 ± 0.49		$0.57^{+0.06}_{-0.03}$
Norm ₂ (BB; 10^{-2})				1.37 ± 1.66		$^c 3.6^{+2.3}_{-2.2} / ^d 4.8^{+2.8}_{-2.8}$
Flux	62	313	168	71	$168^e / 184^f$	$76^e / 87^f$

NOTE. — The fitting models: BB - Blackbody; PL - power-law. The spectral extraction area has a radius of ~ 3 arcmin in Suzaku image larger than that (40 arcsec) in *XMM-Newton* image; Quoted uncertainties are at 90% confidence level. ^a Spectra obtained from the Suzaku. ^b Spectra obtained from the joint *XMM-Newton* and Suzaku. ^c fitting parameters to the *XMM-Newton*. ^d fitting parameters to the Suzaku. ^e 1-10keV (10^{-13} ergs s $^{-1}$ cm $^{-2}$) intrinsic flux from the *XMM-Newton*. ^f 1-10keV (10^{-13} ergs s $^{-1}$ cm $^{-2}$) intrinsic flux from the Suzaku.

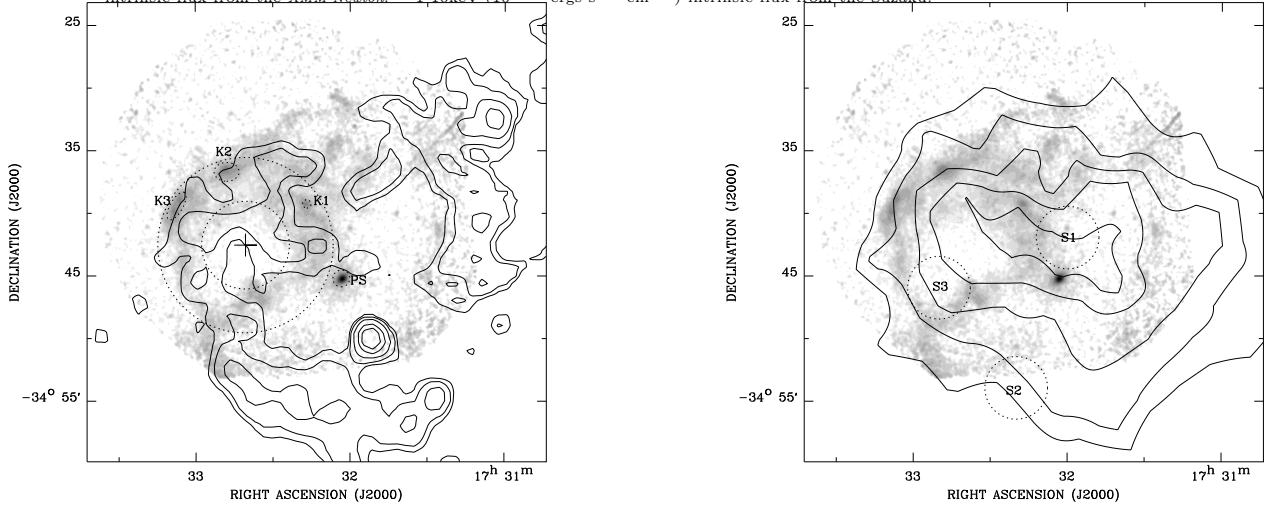


FIG. 1.— Smoothed *XMM-Newton* 0.8-7 keV intensity (greyscale) images overlaid with contours of the VLA radio continuum emission (a) and HESS γ ray emission (b), respectively. The greyscale is logarithmically coded between $(0.5-250) \times 10^{-4}$ cts s $^{-1}$ arcmin $^{-2}$. a: The region enclosed by the two dotted circles outlines the ring-like feature, while the small ellipse /circle outline the bright knots (K1, K2 and K3) and the compact source (CS). b: The circles show the regions where the CO spectra are extracted from.

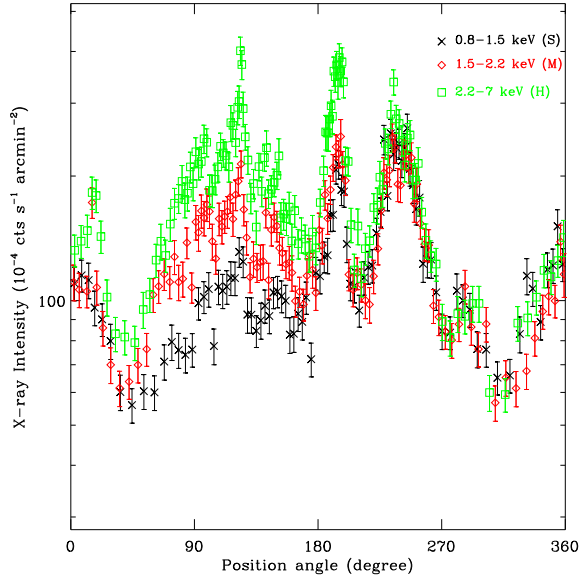


FIG. 2.— Azimuthal X-ray intensity distributions of the ring, extracted from an annulus, with inner-to-outer radii of $3'5-7'$, centering at a position marked by a cross in Fig. 1a. Position angles are measured counterclockwise from south.

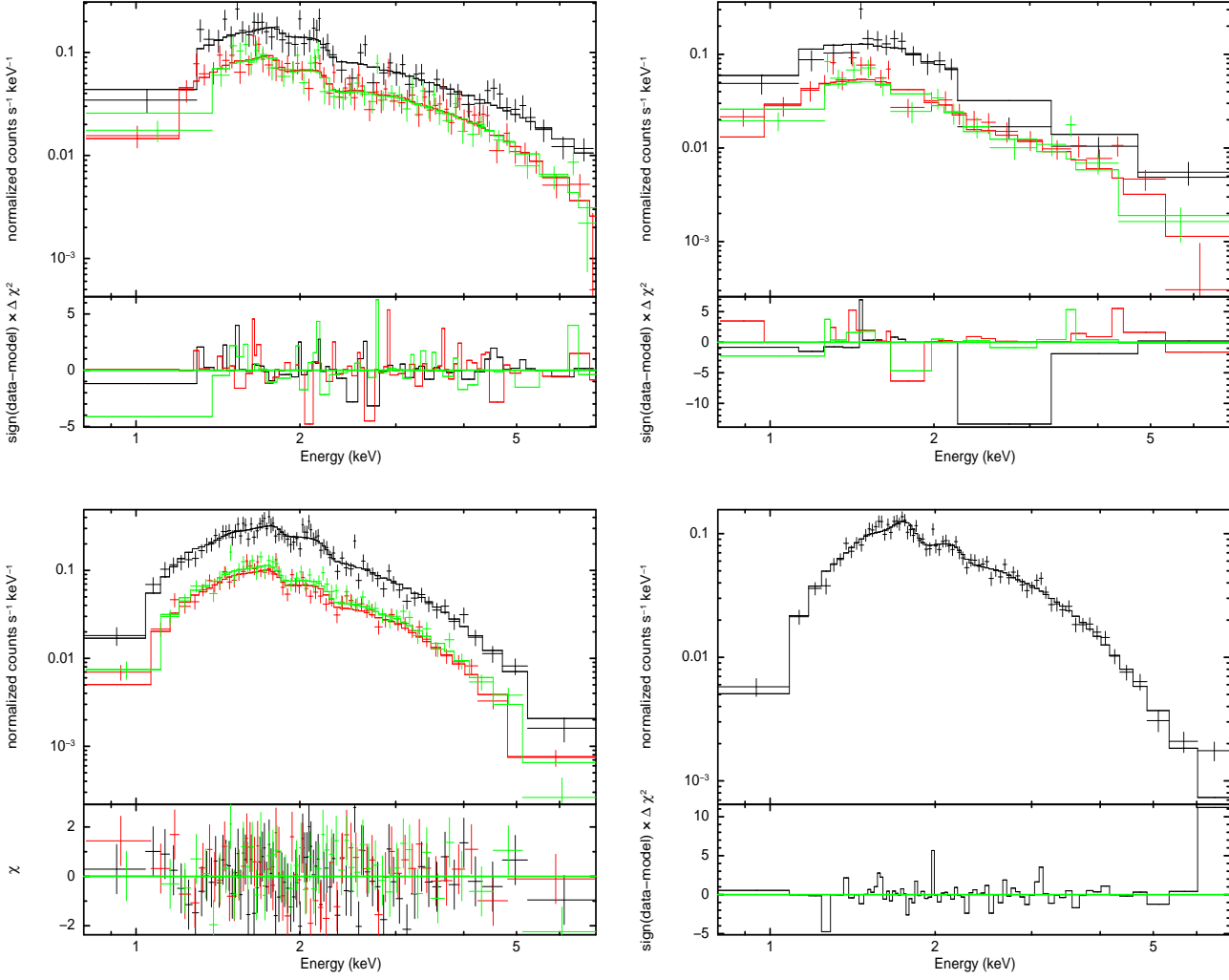


FIG. 3.— Spectra (black: EPIC-pn or Suzaku XIS (right panel of bottom row); red: EPIC-MOS1; green: EPIC-MOS2) extracted from the western ring (left panel of the first row), the eastern ring (right panel of the first row) and the compact source (bottom row) and the best-fit models (see text). The *XMM-Newton* spectra are binned to achieve a signal-to-noise ratio greater than 4 and a minimum of 30 counts per bin, while the *Suzaku* spectrum is binned with a minimum of 100 counts.

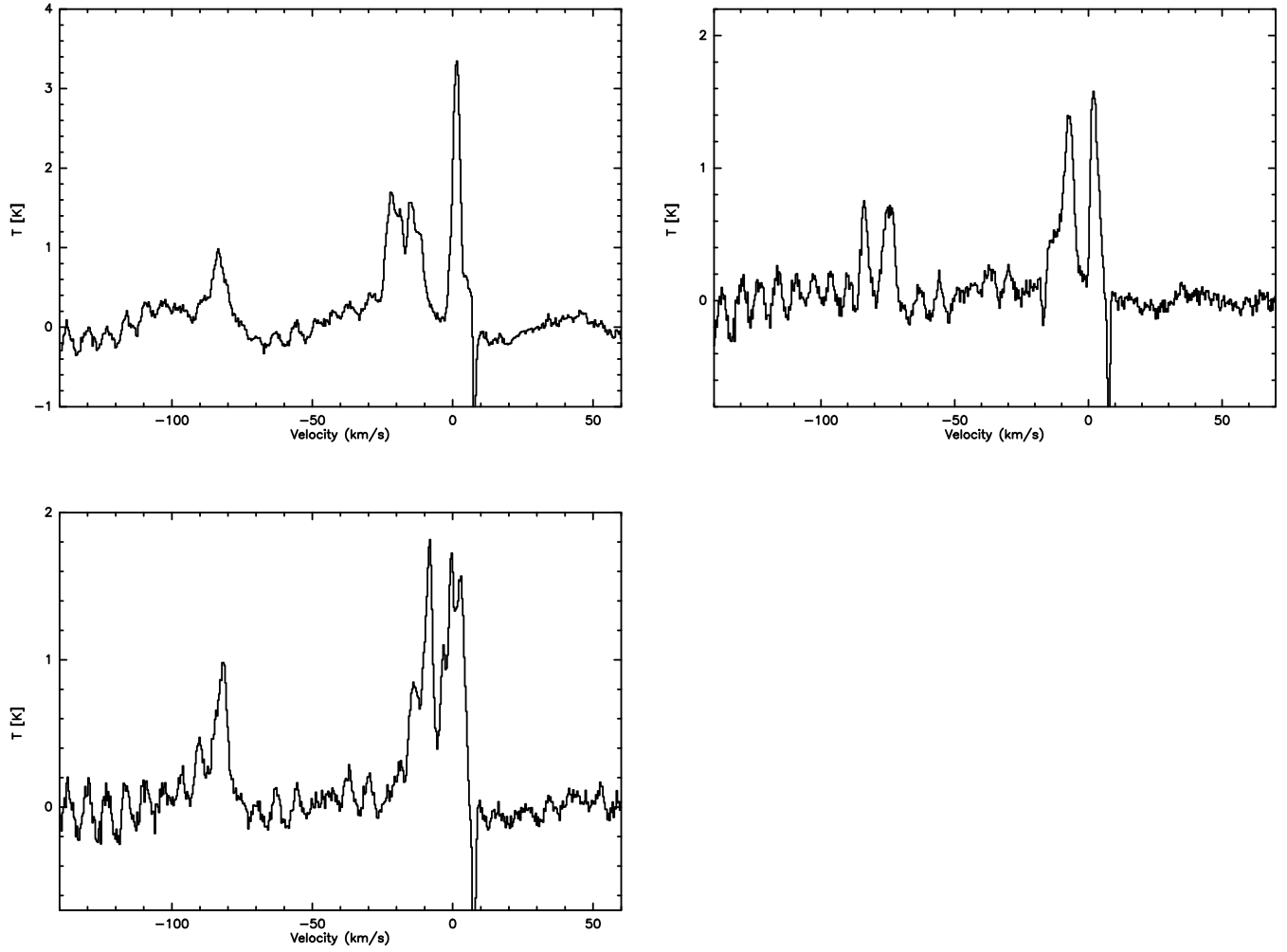


FIG. 4.— The CO spectra from the TeV source peak (S1: the left panel of the first row) and the X-ray peak sites (S3: right of the first row; S2: the bottom row)